Research Article | Vol. 29, No. 20 / 27 Sep 2021 / Optics Express 31488
Optics EXPRESS

Tunable dual-band and high-quality-factor perfect absorption based on VO_2-assisted metasurfaces

SHIWANG YU,[1] ZHANCHENG LI,[1,4] WENWEI LIU,[1] HUA CHENG,[1,5] YUEBIAN ZHANG,[1] BOYANG XIE,[1] WENYUAN ZHOU,[1] JIANGUO TIAN,[1] AND SHUQI CHEN[1,2,3,6]

[1]*The Key Laboratory of Weak Light Nonlinear Photonics, Ministry of Education, Renewable Energy Conversion and Storage Center, School of Physics and TEDA Institute of Applied Physics, Nankai University, Tianjin 300071, China*
[2]*The Collaborative Innovation Center of Extreme Optics, Shanxi University, Taiyuan, Shanxi 030006, China*
[3]*Collaborative Innovation Center of Light Manipulations and Applications, Shandong Normal University, Jinan 250358, China*
[4]*zcli@nankai.edu.cn*
[5]*hcheng@nankai.edu.cn*
[6]*schen@nankai.edu.cn*

Abstract: Perfect absorbers with high quality factors (Q-factors) are of great practical significance for optical filtering and sensing. Moreover, tunable multiwavelength absorbers provide a multitude of possibilities for realizing multispectral light intensity manipulation and optical switches. In this study, we demonstrate the use of vanadium dioxide (VO_2)-assisted metasurfaces for tunable dual-band and high-quality-factor perfect absorption in the mid-infrared region. In addition, we discuss the potential applications of these metasurfaces in reflective intensity manipulation and optical switching. The Q-factors of the dual-band perfect absorption in the proposed metasurfaces are greater than 1000, which can be attributed to the low radiative loss induced by the guided-mode resonances and low intrinsic loss from the constituent materials. By utilizing the insulator–metal transition in VO_2, we further proved that a continuous tuning of the reflectance with a large modulation depth (31.8 dB) can be realized in the designed metasurface accompanied by a dual-channel switching effect. The proposed VO_2-assisted metasurfaces have potential applications in dynamic and multifunctional optical devices, such as tunable multiband filters, mid-infrared biochemical sensors, optical switches, and optical modulators.

1. Introduction

Metasurfaces are planar arrays composed of artificial nanostructures on a subwavelength scale, which have shown unprecedented capabilities to manipulate the amplitude, phase, and polarization of optical waves [1–3]. Owing to the extensive and rapid development of metasurfaces, they have emerged as a versatile platform for the implementation of integrated, miniaturized, and intelligentized optical devices [4]. Latest developments on metasurfaces show their importance in a series of key applications in nanophotonics, such as full-Stokes polarization cameras, high-performance structural color, and aberration-corrected three-dimensional positioning [5–7]. Although metasurfaces have achieved great success, the metasurfaces in most previous studies were static in nature, resulting in fixed optical functionalities. Compared to passive metasurfaces, tunable metasurfaces whose optical functionalities can be dynamically manipulated in both the space and time domains have attracted increasing attention from researchers in both nanophotonics and other disciplines [8]. Owing to the rapid development and application of artificial intelligence

#436046 https://doi.org/10.1364/OE.436046
Journal © 2021 Received 8 Jul 2021; revised 7 Sep 2021; accepted 7 Sep 2021; published 16 Sep 2021

Optics EXPRESS

in nanophotonics, the design and investigation of tunable metasurfaces will open new horizons for the development of self-adaptive and intelligent optical devices [9,10].

Using active materials as the constituent materials of metasurfaces is a common and effective approach to realize tunable metasurfaces. For example, biased diodes are widely used in the gigahertz region; semiconductors and perovskites are mainly used in the terahertz region; and two-dimensional (2D) materials, liquid crystals, germanium antimony telluride (GST), and vanadium oxide (VO_2) are widely used in the visible and infrared regions [11]. By applying different external stimuli, such as heating/cooling, mechanical actuation, and optical pulses, a large contrast in the optical constants of the active materials can be produced, which results in a significant modulation of the optical responses of metasurfaces. As a strongly correlated electron phase-transition material, VO_2 plays an important role in the evolution of tunable metasurfaces. In VO_2, the insulator–metal phase transition at approximately 68 °C causes a significant change in its dielectric permittivity. Because the phase transition in VO_2 can be driven by different external stimuli such as heating/cooling, light pulses, and intense electromagnetic fields, the VO_2-assisted metasurfaces have emerged as an appealing alternative to realize the dynamic manipulation of optical waves [11,12]. In recent advances, VO_2-assisted metasurfaces have been widely used to realize optical modulators, dynamic light focusing, switchable chirality, and tunable perfect absorption [13–27]. In particular, continuous reflectance tuning and switchable perfect absorption based on VO_2-assisted metasurfaces have attracted great interest owing to their flexible and reconfigurable performances [21–25]. For example, by integrating VO_2 into a metasurface plasmonic absorber structure, Liu et al. experimentally demonstrated an electrically active metasurface in the mid-infrared region, which can be used for continuous reflectance spectrum tuning and switchable absorption [28]. However, owing to the high intrinsic loss of plasmonic absorbers, the absorption spectra in several previous studies are typically broadband [21–27]. Tunable perfect absorption with high Q-factors based on VO_2-assisted metasurfaces, which is important for high-performance biosensors, narrowband filters, and infrared spectroscopy [29–32], has not yet been explored.

In this study, we theoretically and numerically demonstrated tunable perfect absorption with high Q-factors in a designed VO_2-assisted metasurface. The absorption peaks with near-unity absorptance at 3049.9 and 3604.2 nm are validated by both simulated and theoretical results, and the Q-factors of these two peaks are 1112.8 and 1381.1, respectively. The high-quality-factor perfect absorption in the proposed design is mainly attributed to the low radiative loss induced by the guided-mode resonances and low intrinsic loss from the constituent materials. A continuous tuning of the reflectance can be realized in the designed metasurface by utilizing the thermally induced insulator–metal transition in VO_2. Therefore, the proposed VO_2-assisted metasurface can be used as a dual-channel ultra-narrow-band optical switch, in which the reflectance modulation depths are 16.1 and 31.8 dB at 3049.9 and 3604.2 nm, respectively. We further demonstrate a dual-band optical switch with opposite switching characteristics ("on" or "off") at two working wavelengths by adjusting one of the structural parameters. Numerical analysis also shows that multiband and high-quality-factor absorption can be implemented in the designed metasurface for oblique transverse magnetic (TM) polarized illumination. Our study reveals the underlying physics of the realization of VO_2-assisted-metasurface-based tunable high-quality-factor perfect absorption, which provides useful guidance for researches on tunable optical devices with high Q-factors.

2. Results and discussion

Figure 1(a) illustrates the active manipulation of the optical responses of the designed VO_2-assisted metasurface. The metasurface can be treated as a perfect absorber at 60°C, partial reflector at 70°C, and highly efficient reflector at 88°C. Moreover, the continuous tuning of the reflectance can be implemented in the designed metasurface by utilizing the thermally induced insulator–metal

Optics EXPRESS

transition in VO_2. Figure 1(b) schematically illustrates the unit cell of the proposed metasurface. The designed VO_2-assisted metasurface consists of VO_2 nanodisks, an amorphous silicon (a-Si) layer, aluminum oxide (Al_2O_3) dielectric layer, and aluminum layer. The structural parameters of the designed metasurface were: $p = 1300$ nm, $S = d/p = 0.3$, $t_1 = 400$ nm, $t_2 = 500$ nm, and $t_3 = 250$ nm. Furthermore, the thickness of the aluminum layer was set to 300 nm to ensure zero transmittance. The finite-difference time-domain (FDTD) method was used to simulate, analyze, and explore the characteristics of the designed metasurface. In the simulation, the refractive index of Al_2O_3 was taken as 1.70, and the optical constants of aluminum in the mid-infrared region obtained by linear interpolation of the experimental data were used [33]. VO_2 was simulated using thermally tunable relative permittivity [34]. The dielectric constants of a-Si were obtained from Palik′s Handbook [35].

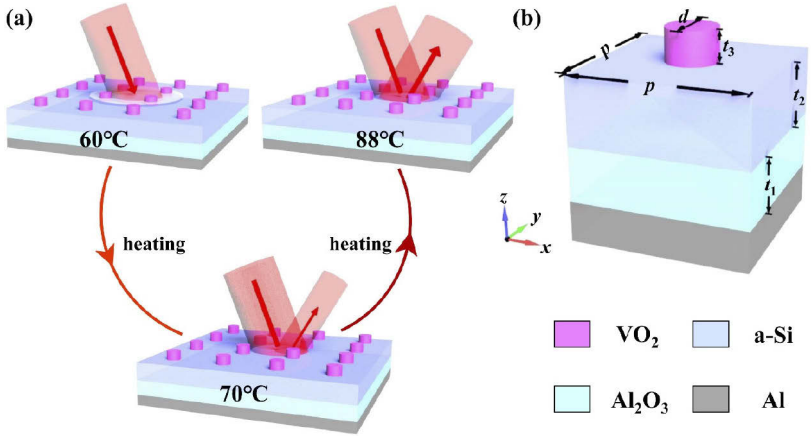

Fig. 1. Schematic representation of the designed VO_2-assisted metasurface. (a) Artistic rendering of the continuous reflectivity modulation in the designed metasurface using the thermally induced insulator–metal transition in VO_2. (b) Schematic representation of the structure of a unit cell of the designed metasurfaces.

To illustrate the high-quality-factor perfect absorption in the designed VO_2-assisted metasurfaces, we first simulated the absorption spectrum under TM-polarized normal illumination at 60 °C, as shown in Fig. 2(a). The absorption peaks with near-unity absorptance (over 97.70%) were observed at $\lambda_1 = 3049.9$ nm and $\lambda_2 = 3604.2$ nm, and the Q-factors of these two peaks were 1112.8 and 1381.1, respectively. The perfect absorption in the proposed metasurface is polarization-independent for normal incidence because the VO_2 nanodisk in the unit cell is isotropic in both the x and y directions. Meanwhile, we utilized the coupled mode theory (CMT) to further describe the input–output properties of the designed metasurface. Owing to the existence of the aluminum layer, the designed metasurface can be viewed as a single-port system, in which the transmittance is equal to zero. Accordingly, the absorption of the designed system can be characterized by the CMT [36,37]:

$$A = 1 - R = \frac{4\delta\gamma}{(\omega - \omega_0)^2 + (\delta + \gamma)^2}. \tag{1}$$

Here, δ and γ describe the intrinsic loss rate and external leakage rate of the designed system, respectively, and ω_0 is the resonance frequency. According to Eq. (1), perfect absorption can be achieved at the resonance frequency ($\omega = \omega_0$) when the external leakage rate and intrinsic loss rate are equal ($\delta = \gamma$), which is known as the critical coupling. As shown in Fig. 2(b), the fitted absorption spectra using the CMT and the simulated absorption spectra are consistent, which suggests that the CMT can provide a reasonable elucidation of the designed metasurface.

Optics EXPRESS

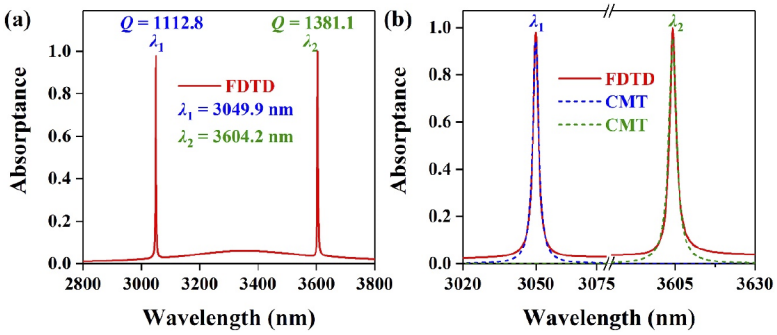

Fig. 2. Dual-band and high-quality-factor perfect absorption in the designed VO_2-assisted metasurface. (a) Simulated absorption spectrum of the proposed VO_2-assisted metasurface under TM-polarized normal illumination at 60°C, and (b) theoretically fitted results using the CMT for resonance wavelengths $\lambda_1 = 3049.9$ nm and $\lambda_2 = 3604.2$ nm.

Meanwhile, for this single-port system, the effective impedance of the absorber can be expressed as [38,39]

$$Z = \sqrt{\frac{(1+S_{11})^2}{(1-S_{11})^2}}. \tag{2}$$

Here, S_{11} is the complex reflection coefficient of a single port. To achieve total absorption, the reflection must be completely suppressed (that is, $|S_{11}| = 0$). This corresponds to perfect impedance matching, that is, $Z = Z_0 = 1$, where Z_0 is the effective impedance of the free space. Therefore, the calculated effective impedances of the designed metasurface at the resonance wavelengths λ_1 and λ_2 are $Z_1 = 0.9899 + 0.2944$i and $Z_2 = 0.9701 + 0.0417$i, respectively. These impedances are approximately equal to the effective impedance of the free space, thereby validating the perfect absorption at the two resonance wavelengths.

To reveal the physical mechanism of the high-quality-factor perfect absorption in the designed VO_2-assisted metasurfaces, we simulated the electromagnetic field distributions at the two resonance wavelengths, as shown in Fig. 3(a) and 3(b). The field distributions indicate that typical TM_0 and TE_0 modes of the waveguide are formed at $\lambda_1 = 3049.9$ nm and $\lambda_2 = 3604.2$ nm respectively, which represent the existence of the guided-mode resonances. At 60 °C, VO_2 is in the insulator phase, thus the VO_2 nanodisk array can be viewed as a 2D dielectric grating. Therefore, the VO_2 nanodisks and the a-Si waveguide layer as a whole can be regarded as a typical resonant waveguide grating. It causes coupling between the incident light and the a-Si layer where most of the fields are localized [40,41]. Thereafter, most of the localized field energy is absorbed by the bottom aluminum layer, and the rest is consumed by the upper VO_2 disks and a-Si layer. The high-quality-factor perfect absorption in the designed VO_2-assisted metasurfaces can be attributed to the low radiative loss and low intrinsic loss [42]. The guided-mode resonances with low radiative loss are excited, and the extremely small extinction coefficient of the VO_2 and a-Si induces a low intrinsic loss. Meanwhile, the electromagnetic fields near the aluminum layer are relatively small, which also results in a low intrinsic loss. In addition, utilizing a multilayer dielectric Bragg reflector instead of a lossy metal film may produce a higher Q-factor owing to its reduced intrinsic loss, which will also cause the structure to become thicker [37,38].

The high-quality-factor near-perfect absorption in the designed metasurfaces is directly related to the critical coupling induced by the guided-mode resonances. Hence, the variations in the structural parameters d, p, t_1, t_2 and t_3 have a significant effect on the excitation of the guided-mode resonances, which will significantly change the absorption characteristic of the designed metasurface. We further analyzed the influence of the structural parameters on the

Optics EXPRESS

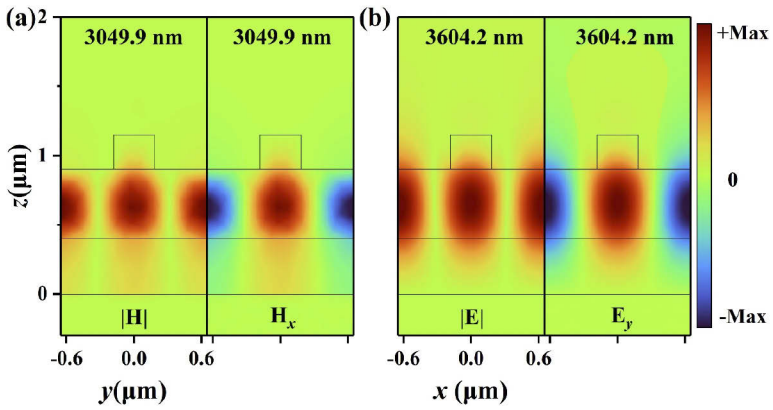

Fig. 3. Guided-mode resonances in the designed VO_2-assisted metasurface. (a) Simulated results of the distribution of the magnetic field intensity ($|\mathbf{H}|$) and the real part of the magnetic field components H_x in the y–z plane at the resonance wavelength $\lambda_1 = 3049.9$ nm. (b) Simulated results of the distribution of the electric field intensity ($|\mathbf{E}|$) and the real part of the electric field component E_y in the x–z plane at the resonance wavelength $\lambda_2 = 3604.2$ nm.

absorption spectrum of the designed metasurface to determine the physical mechanism. The simulated results are presented in Fig. 4. With the increase of the ratio S (representing the increase in d), the external leakage rate γ significantly increased, while the intrinsic loss rate δ is slightly affected (owing to the extremely small extinction coefficient of VO_2 at 60 °C). Consequently, a transition from undercoupling ($S = 0.20$) through critical coupling ($S = 0.30$) to overcoupling ($S = 0.40$, 0.50) can be observed in Fig. 4(a), where the near-unity absorptances are achieved at the critical coupling condition and the larger or smaller S parameters will cause the absorptances to go down [37,43]. The variation trends of the absorption spectra with the changes in p and t_2 are analogous, as shown in Fig. 4(b) and 4(d). The linewidths of the absorption peaks remain unchanged owing to the relative stability of both external leakage rate γ and intrinsic loss rate δ with variations in p and t_2. Meanwhile, the two resonant peaks undergo a redshift with the increase of the period p and α-Si waveguide thickness t_2. The increase of period p is equivalent to the amplification of the structure perpendicular to the propagation direction (the diameter of VO_2 nanodisks $d = S * p$, here, S is constant), which causes the resonant wavelengths to increase. The phase matching condition between the incident light and a lateral waveguide mode will be satisfied at a longer wavelength when the α-Si waveguide thickness t_2 is increased, leading to the redshift of the resonant wavelengths for guided-mode resonances [41].

Differently, as shown in Fig. 4(c), owing to the fact that guided-mode resonances are weakly perturbed by the depth of upper VO_2 grating for the proposed structure, the resonance peak positions and efficiencies show good robustness to changes in thickness t_3. The results in Fig. 4(e) indicate that the absorptance at the two resonance peaks reaches a maximum when $t_1 = 400$ nm, for which critical coupling is induced. Correspondingly, undercoupling and overcoupling are produced for $t_1 = 300$ nm and $t_1 = 500$ nm, respectively, resulting in a decrease in the absorptance. The intrinsic loss rate δ decreases with the increase of the Al_2O_3 dielectric layer thickness t_1, while the external leakage rate γ is relatively robust [44]. As a result, the Q-factors of the absorption peaks become higher with the increase of t_1. In fact, the dispersion of the extinction coefficient from the constituent materials in the wavelength region also affects the intrinsic loss rate δ. This effect can be ignored within a certain range of parameter changes, according to the simulation results.

Optics EXPRESS

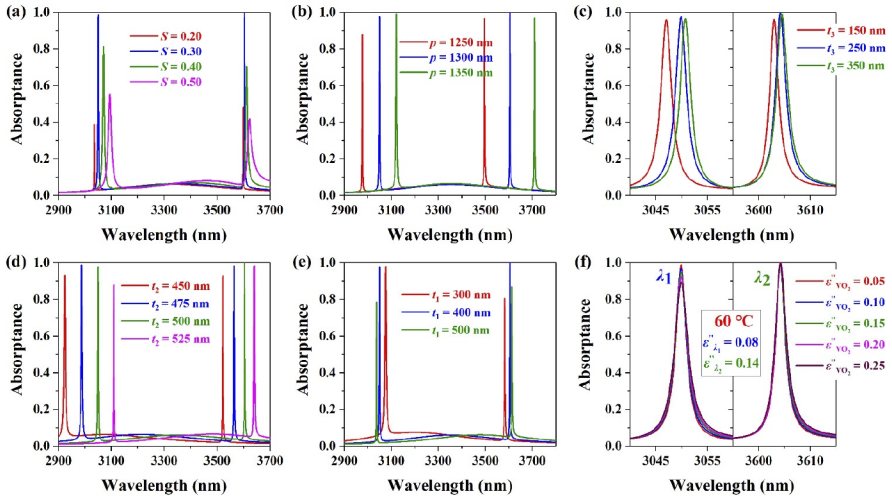

Fig. 4. Effect of the structural parameters and material losses on the absorption spectrum of the designed VO_2-assisted metasurface. Change in the absorption spectra under TM-polarized normal illumination with respect to (a) S (defined as the ratio between the diameter d of the VO_2 disks and the period p of a unit cell), (b) period p, (c) height t_3 of the VO_2 nanodisk (d) thickness t_2 of the a-Si layer, and (e) thickness t_1 of the Al_2O_3 dielectric layer at 60°C. (f) Change in the absorption spectra under TM-polarized normal illumination at 60°C when varying the imaginary part of the relative permittivity (ε'') of VO_2. The material parameters in the black box represent the ε'' values of VO_2 at resonance wavelengths λ_1 and λ_2 used in the above simulation. Except for the interested parameters, the other structural parameters remain unchanged.

To verify the feasibility of the experiment, we further analyzed the effects of higher material loss of fabricated sample on the absorptances at the resonance wavelengths. As shown in Fig. 4(f), when the imaginary part of the relative permittivity of VO_2 increases from 0.05 to 0.25, the near-perfect absorption can still be achieved at $\lambda_2 = 3604.2$ nm and over 89.5% absorptances can be maintained at $\lambda_1 = 3049.9$ nm, which show the robustness of the proposed structure to material loss. As a matter of fact, the loss of VO_2 in the dielectric phase can be further reduced by cooling the structure. The results shown in Fig. 4 further validate the physical mechanism presented in this study.

Using the thermally induced insulator–metal transition in VO_2, the critical coupling caused by the guided-mode resonances in the designed metasurface can be dynamically manipulated, thereby resulting in the active control of the absorption characteristic of the designed metasurface. To display the dynamic manipulation capability of the designed metasurface, we simulated the absorption spectra of the designed metasurface at different temperatures, as shown in Fig. 5(a). The results indicate that thermally induced continuous tuning of the absorptance is achieved at the resonant wavelengths λ_1 and λ_2, which can be attributed to the disruption of the balance between the radiative loss and the intrinsic loss. With the increase in the temperature, VO_2 gradually transmits from the dielectric phase to the metallic phase, resulting in substantial changes in both real and imaginary parts of its permittivity. The phase transition induces a gradual reduction of the refractive indices of VO_2, to some extent, resulting in less incident light is coupled into the α-Si waveguide layer. More importantly, a higher intrinsic loss is produced as the extinction coefficient of VO_2 increases significantly, leading to larger resonance widths (lower Q-factors). The thermally induced continuous tuning of the absorptance in the designed metasurfaces is equivalent to a continuous tuning of the reflectance because the sum of the absorptance and

Optics EXPRESS

reflectance is equal to 1. It is worth mentioning that switching between broadband reflection and absorption beyond 80% absorption efficiency with raising the temperature from 60 °C to 88 °C, as shown by the gray shaded area in Fig. 5(a). At 88°C, VO_2 is in the metal phase, a vertical Fabry Perot-like mode is formed between the upper metal-phase VO_2 and bottom Al metallic layer due to the higher thickness of the spacer layer (α-Si and Al_2O_3) [2,45]. As a result, the field enhancement is mainly concentrated near upper VO_2 and the incident light is mainly absorbed by the VO_2, resulting in the broadband high-efficiency absorption. In addition, as shown in Fig. 5(a) and 5(b), the designed metasurface can be considered as a dual-channel optical switch with the "off/off" state at 60°C and "on/on" state at 88 °C. Here, the "off" and "on" states correspond to high absorption and reflection rates, respectively. The reflectance increases from −16.5 dB (A = 97.74%) to −0.4 dB (R = 91.63%) at $\lambda_1 = 3049.9$ nm and from −32.7 dB (A = 99.95%) to −0.9 dB (R = 80.84%) at $\lambda_2 = 3604.2$ nm with the increase in the temperature from 60°C to 88°C. This result in the large modulation depths of 16.1 dB at λ_1 and 31.8 dB (approximately three orders of reflection modulation depth) at λ_2. To the best of our knowledge, more than three orders of reflection modulation depth have not yet been reported for VO_2-assisted metasurfaces.

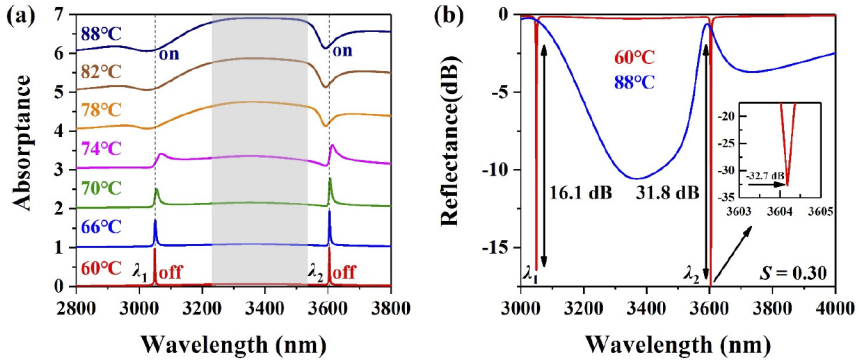

Fig. 5. Implementation of continuous reflectivity modulation based on the designed VO_2-assisted metasurface by utilizing the thermally induced insulator–metal transition in VO_2. (a) The absorption spectra of the designed metasurface under TM-polarized normal illuminations at different temperatures with $S = 0.30$. The gray dashed lines represent the positions of the two resonance wavelengths at 60°C at the wavelengths $\lambda_1 = 3049.9$ nm and $\lambda_2 = 3604.2$ nm. Moreover, the gray shaded area represents a tunable broadband absorption. (b) The reflection spectra of the designed metasurface under TM-polarized illuminations at 60°C (insulator phase) and 88°C (metallic phase), respectively. The inset shows the reflectance at $\lambda_2 = 3604.2$ nm.

In the designed metasurface, the critical coupling induced by the guided-mode resonances can be realized under different working wavelengths at a fixed temperature and different resonant wavelengths at different temperatures by changing the structural parameter S. As shown in Fig. 6, a dual-band optical switch with opposite switching characteristics ("on" or "off") at two working wavelengths can be obtained for $S = 0.75$. The results in Fig. 6(a) indicate that the designed metasurface achieves critical coupling at the resonance wavelengths $\lambda_1 = 2564.1$ nm ($Q = 102.6$) and $\lambda_2 = 3173.6$ nm ($Q = 46.9$) at 60°C and 70 °C, respectively. As a result, a switching effect between the "off/on" and "on/off" states are produced when the temperature increases from 60 °C to 70 °C for wavelengths λ_1 and λ_2. The same switching effect also occurs at 60°C and 78°C for $\lambda_1 = 2564.1$ nm and $\lambda_3 = 3260.3$ nm, respectively. Moreover, as shown in Fig. 6(b), for the working temperatures of 60°C and 70°C (or 78°C), the reflectance extinction ratios of 20.1 dB (21.3 dB) and 29.5 dB (34.5 dB) are achieved at λ_1 and λ_2 (λ_3) respectively, which represent significantly high modulation depth. It is worth mentioning that the phase transition in VO_2

Optics EXPRESS

can also be triggered by ultrafast laser pulses, and the time for switching between the two states of VO_2 can be in the sub-picosecond range. Thus, given this fact, it can be expected that the designed metasurface may provide useful guidance for achieving high-performance ultrafast active devices.

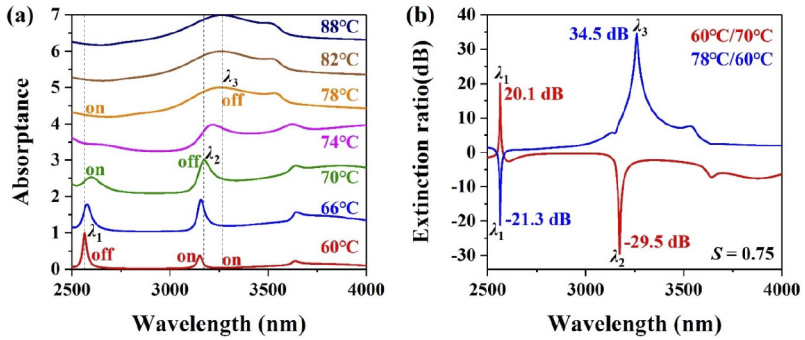

Fig. 6. Dual-band optical switch based on the designed VO_2-assisted metasurface. (a) Simulated results of the absorption spectra of the designed metasurface under TM-polarized normal illuminations at different temperatures with $S = 0.75$. The gray dashed lines represent the positions of the three working wavelengths: $\lambda_1 = 2564.1$ nm, $\lambda_2 = 3173.6$ nm, and $\lambda_3 = 3260.3$ nm. (b) Simulated results of the extinction ratio (ER) of the reflectance between 60°C and 70°C (or 78°C and 60°C) with $S = 0.75$. $\mathrm{ER} = -10\log_{10}(R_2 / R_1)$, where R_2 and R_1 are the reflectances at the corresponding temperatures.

Because the excitation of the guided-mode resonances is sensitive to the incident angle [46], the absorption characteristics of the designed metasurface were further investigated at different

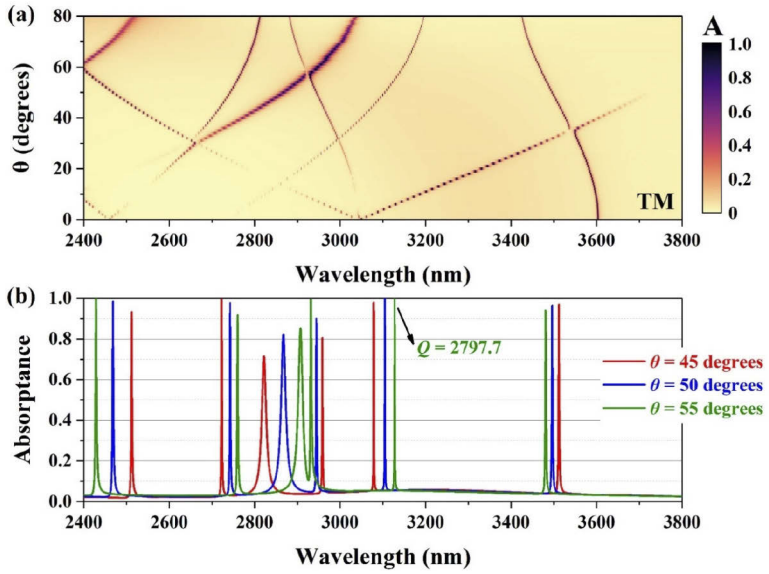

Fig. 7. Angle-sensitive multiband and high-quality-factor absorption in the designed VO_2-assisted metasurface. (a) Change in the absorption spectra of the designed metasurface ($S = 0.30$) under different incident angles of TM-polarized illumination at 60°C. (b) Simulated results of the absorption spectra (at 60°C) of the designed metasurface ($S = 0.30$) under TM-polarized illumination with incident angles equal to 45°, 50°, and 55°.

Optics EXPRESS

incident angles, as shown in Fig. 7. In contrast to previous perfect absorbers based on plasmonic metasurfaces, whose optical responses are robust to the incident angle, the absorption peaks of the designed metasurface exhibit a rapid variation with respect to the incident angle, which acts as a separation of resonances. This is because the resonances are degenerate at normal incidence, whereas a non-zero incident angle can remove this degeneration. The observed separation of the resonance peaks in Fig. 7(a) represents a type of typical inherent resonant characteristic that has also been reported in other nanostructures by previous studies [37,47,48]. As shown in Fig. 7(b), multiple-wavelength and high-quality- factor absorption can be realized in the designed metasurface under TM-polarized illumination with larger incident angles. For example, five peaks with approximately 90% absorptance can be observed for the incident angle $\theta = 55°$, and three of them achieve near-perfect absorption with the absorptance of over 99%. In particular, an absorption peak with a maximum Q-factor of 2797.7 appears at 3127.5 nm. Because of the existence of atmospheric transparency windows and molecular vibrational fingerprints in the mid-infrared spectral region, the multiple-wavelength and high-quality-factor absorption in the designed metasurface may facilitate mid-infrared biochemical sensing and thermal imaging.

3. Conclusions

We proposed VO_2-assisted metasurfaces to realize tunable dual-band and high-quality-factor perfect absorption in the mid-infrared region. Both simulated and theoretical results validate the existence of two absorption peaks with near-unity absorptance at 3049.9 and 3604.2 nm, whose Q-factors were 1112.8 and 1381.1, respectively. The high-quality-factor perfect absorption in the proposed design was mainly attributed to the low radiative loss induced by the guided-mode resonances and the low intrinsic loss from the constituent materials. We demonstrated that the continuous tuning of the reflectance can be realized in the designed metasurface by utilizing the thermally induced insulator–metal transition in VO_2. As a result, the proposed design can be used as a dual-channel ultra-narrow-band optical switch, in which the reflectance modulation depth is 16.1 and 31.8 dB at 3049.9 and 3604.2 nm, respectively. By varying the ratio S, we obtained a dual-band optical switch with opposite switching characteristics at two working wavelengths. The angle-sensitive multiband and high-quality-factor absorption in the designed metasurface under oblique TM-polarized illumination has also been discussed. This study reveals the potential use of the VO_2-assisted metasurfaces in tunable narrow-band reflective intensity manipulation and optical switches, which provides useful guidance for researches on tunable multispectral optical devices with high Q-factors.

Funding. National Key Research and Development Program of China (2017YFA0303800, 2016YFA0301102); Natural Science Foundation of Tianjin for Distinguished Young Scientists (18JCJQJC45700); National Natural Science Foundation of China (11774186, 11904181, 11904183, 11974193, 91856101); National Natural Science Fund for Distinguished Young Scholar (11925403); China Postdoctoral Science Foundation (2018M640224, 2021M690084).

Disclosures. The authors declare no conflicts of interest.

Data availability. Data underlying the results presented in this paper are not publicly available at this time but may be obtained from the authors upon reasonable request.

References

1. K. Koshelev and Y. Kivshar, "Dielectric resonant metaphotonics," ACS Photonics **8**(1), 102–112 (2021).
2. S. Sun, Q. He, J. Hao, S. Xiao, and L. Zhou, "Electromagnetic metasurfaces: physics and applications," Adv. Opt. Photonics **11**(2), 380–479 (2019).
3. Z. Li, W. Liu, H. Cheng, and S. Chen, "Few-layer metasurfaces with arbitrary scattering properties," Sci. China Phys. Mech. **63**(8), 1–12 (2020).
4. S. Chen, W. Liu, Z. Li, H. Cheng, and J. Tian, "Metasurface-Empowered Optical Multiplexing and Multifunction," Adv. Mater. **32**(3), 1805912 (2020).
5. N. A. Rubin, G. D'Aversa, P. Chevalier, Z. Shi, W. T. Chen, and F. Capasso, "Matrix Fourier optics enables a compact full-Stokes polarization camera," Science **365**(6448), eaax1839 (2019).
6. W. Yang, S. Xiao, Q. Song, Y. Liu, Y. Wu, S. Wang, J. Yu, J. Han, and D. P. Tsai, "All-dielectric metasurface for high-performance structural color," Nat. Commun. **11**(1), 1864 (2020).

Optics EXPRESS

7. W. Liu, D. Ma, Z. Li, H. Cheng, D. Y. Choi, J. Tian, and S. Chen, "Aberration-corrected three-dimensional positioning with a single-shot metalens array," Optica **7**(12), 1706–1713 (2020).
8. A. M. Shaltout, V. M. Shalaev, and M. L. Brongersma, "Spatiotemporal light control with active metasurfaces," Science **364**(6441), eaat3100 (2019).
9. P. Thureja, G. K. Shirmanesh, K. T. Fountaine, R. Sokhoyan, M. Grajower, and H. A. Atwater, "Array-Level Inverse Design of Beam Steering Active Metasurfaces," ACS Nano **14**(11), 15042–15055 (2020).
10. S. Zhang, "AI empowered metasurfaces," Light: Sci. Appl. **9**(1), 94 (2020).
11. Q. He, S. Sun, and L. Zhou, "Tunable/reconfigurable metasurfaces: physics and applications," Research **2019**, 1849272 (2019).
12. K. Liu, S. Lee, S. Yang, O. Delaire, and J. Wu, "Recent progresses on physics and applications of vanadium dioxide," Mater. Today **21**(8), 875–896 (2018).
13. Z. Lin, L. Huang, R. Zhao, Q. Wei, T. Zentgraf, Y. Wang, and X. Li, "Dynamic control of mode modulation and spatial multiplexing using hybrid metasurfaces," Opt. Express **27**(13), 18740–18750 (2019).
14. X. Duan, S. T. White, Y. Cui, F. Neubrech, Y. Gao, R. F. Haglund, and N. Liu, "Reconfigurable Multistate Optical Systems Enabled by VO_2 Phase Transitions," ACS Photonics **7**(11), 2958–2965 (2020).
15. P. B. Savaliya, A. Thomas, R. Dua, and A. Dhawan, "Tunable optical switching in the near-infrared spectral regime by employing plasmonic nanoantennas containing phase change materials," Opt. Express **25**(20), 23755–23772 (2017).
16. Z. Zhu, P. G. Evans, R. F. Haglund Jr, and J. G. Valentine, "Dynamically reconfigurable metadevice employing nanostructured phase-change materials," Nano Lett. **17**(8), 4881–4885 (2017).
17. R. Ji, Y. Hua, K. Chen, K. Long, Y. Fu, X. Zhang, and S. Zhuang, "A switchable metalens based on active tri-layer metasurface," Plasmonics **14**(1), 165–171 (2019).
18. S. Wang, L. Kang, and D. H. Werner, "Active terahertz chiral metamaterials based on phase transition of vanadium dioxide (VO_2)," Sci. Rep. **8**(1), 1–9 (2018).
19. M. Liu, E. Plum, H. Li, S. Duan, S. Li, Q. Xu, X. Zhang, C. Zhang, C. Zou, B. Jin, J. Han, and W. Zhang, "Switchable Chiral Mirrors," Adv. Opt. Mater. **8**(15), 2000247 (2020).
20. J. Luo, X. Shi, X. Luo, F. Hu, and G. Li, "Broadband switchable terahertz half-/quarter-wave plate based on metal-VO_2 metamaterials," Opt. Express **28**(21), 30861–30870 (2020).
21. T. Lv, G. Dong, C. Qin, J. Qu, B. Lv, W. Li, Z. Zhu, Y. Li, C. Guan, and J. Shi, "Switchable dual-band to broadband terahertz metamaterial absorber incorporating a VO_2 phase transition," Opt. Express **29**(4), 5437–5447 (2021).
22. J. Huang, J. Li, Y. Yang, J. Li, J. Li, Y. Zhang, and J. Yao, "Broadband terahertz absorber with a flexible, reconfigurable performance based on hybrid-patterned vanadium dioxide metasurfaces," Opt. Express **28**(12), 17832–17840 (2020).
23. J. Li, C. Zheng, J. Li, H. Zhao, X. Hao, H. Xu, Z. Yue, Y. Zhang, and J. Yao, "Polarization-dependent and tunable absorption of terahertz waves based on anisotropic metasurfaces," Opt. Express **29**(3), 3284–3295 (2021).
24. D. Yan, M. Meng, J. Li, J. Li, and X. Li, "Vanadium dioxide-assisted broadband absorption and linear-to-circular polarization conversion based on a single metasurface design for the terahertz wave," Opt. Express **28**(20), 29843–29854 (2020).
25. H. He, X. Shang, L. Xu, J. Zhao, W. Cai, J. Wang, C. Zhao, and L. Wang, "Thermally switchable bifunctional plasmonic metasurface for perfect absorption and polarization conversion based on VO_2," Opt. Express **28**(4), 4563–4570 (2020).
26. N. Mou, S. Sun, H. Dong, S. Dong, Q. He, L. Zhou, and L. Zhang, "Hybridization-induced broadband terahertz wave absorption with graphene metasurfaces," Opt Express **26**(9), 11728–11736 (2018).
27. N. Mou, X. Liu, T. Wei, H. Dong, Q. He, L. Zhou, Y. Zhang, L. Zhang, and S. Sun, "Large-scale, low-cost, broadband and tunable perfect optical absorber based on phase-change material," Nanoscale **12**(9), 5374–5379 (2020).
28. L. Liu, L. Kang, T. S. Mayer, and D. H. Werner, "Hybrid metamaterials for electrically triggered multifunctional control," Nat. Commun. **7**(1), 13236 (2016).
29. N. Liu, M. Mesch, T. Weiss, M. Hentschel, and H. Giessen, "Infrared perfect absorber and its application as plasmonic sensor," Nano Lett. **10**(7), 2342–2348 (2010).
30. T. Inoue, M. De Zoysa, T. Asano, and S. Noda, "Realization of narrowband thermal emission with optical nanostructures," Optica **2**(1), 27–35 (2015).
31. H. H. Chen, Y. C. Su, W. L. Huang, C. Y. Kuo, W. C. Tian, M. J. Chen, and S. C. Lee, "A plasmonic infrared photodetector with narrow bandwidth absorption," Appl. Phys. Lett. **105**(2), 023109 (2014).
32. S. Kang, Z. Qian, V. Rajaram, S. D. Calisgan, A. Alù, and M. Rinaldi, "Ultra-Narrowband Metamaterial Absorbers for High Spectral Resolution Infrared Spectroscopy," Adv. Opt. Mater. **7**(2), 1801236 (2019).
33. A. D. Rakić, "Algorithm for the determination of intrinsic optical constants of metal films: application to aluminum," Appl. Opt. **34**(22), 4755–4767 (1995).
34. H. S. Choi, J. S. Ahn, J. H. Jung, T. W. Noh, and D. H. Kim, "Mid-infrared properties of a VO_2 film near the metal-insulator transition," Phys. Rev. B **54**(7), 4621–4628 (1996).
35. E. D. Palik, Handbook of optical constants of solids (Academic Press, 1985).
36. S. Fan, W. Suh, and J. D. Joannopoulos, "Temporal coupled-mode theory for the Fano resonance in optical resonators," J. Opt. Soc. Am. A **20**(3), 569–572 (2003).
37. J. R. Piper and S. Fan, "Total Absorption in a Graphene Monolayer in the Optical Regime by Critical Coupling with a Photonic Crystal Guided Resonance," ACS Photonics **1**(4), 347–353 (2014).

Optics EXPRESS

38. Y. M. Qing, H. F. Ma, Y. Z. Ren, S. Yu, and T. J. Cui, "Near-infrared absorption-induced switching effect via guided mode resonances in a graphene-based metamaterial," Opt. Express **27**(4), 5253–5263 (2019).
39. J. Hao, L. Zhou, and M. Qiu, "Nearly total absorption of light and heat generation by plasmonic metamaterials," Phys. Rev. B **83**(16), 165107 (2011).
40. A. Sharon, S. Glasberg, D. Rosenblatt, and A. A. Friesem, "Metal-based resonant grating waveguide structures," J. Opt. Soc. Am. A **14**(3), 588–595 (1997).
41. G. Quaranta, G. Basset, O. J. F. Martin, and B. Gallinet, "Recent Advances in Resonant Waveguide Gratings," Laser Photonics Rev. **12**(9), 1800017 (2018).
42. J. Tian, Q. Li, P. A. Belov, R. K. Sinha, W. Qian, and M. Qiu, "High-Q All-Dielectric Metasurface: Super and Suppressed Optical Absorption," ACS Photonics **7**(6), 1436–1443 (2020).
43. C. Qu, S. Ma, J. Hao, M. Qiu, X. Li, S. Xiao, Z. Miao, N. Dai, Q. He, S. Sun, and L. Zhou, "Tailor the Functionalities of Metasurfaces Based on a Complete Phase Diagram," Phys. Rev. Lett. **115**(23), 235503 (2015).
44. C. Verlhac, M. Makhsiyan, R. Haidar, J. Primot, and P. Bouchon, "Towards perfect metallic behavior in optical resonant nanostructures," Opt Express **29**(12), 18458–18468 (2021).
45. S. Ma, S. Xiao, and L. Zhou, "Resonant modes in metal/insulator/metal metamaterials: An analytical study on near-field couplings," Phys. Rev. B **93**(4), 045305 (2016).
46. S. S. Wang and R. Magnusson, "Theory and applications of guided-mode resonance filters," Appl. Opt. **32**(14), 2606–2613 (1993).
47. Z. S. Liu, S. Tibuleac, D. Shin, P. P. Young, and R. Magnusson, "High-efficiency guided-mode resonance filter," Opt. Lett. **23**(19), 1556–1558 (1998).
48. C. C. Guo, Z. H. Zhu, X. D. Yuan, W. M. Ye, K. Liu, J. F. Zhang, W. Xu, and S. Q. Qin, "Experimental Demonstration of Total Absorption over 99% in the Near Infrared for Monolayer-Graphene-Based Subwavelength Structures," Adv. Opt. Mater. **4**(12), 1955–1960 (2016).